

---

# Explaining Image Classifiers by Adaptive Dropout and Generative In-filling

---

**Chun-Hao Chang**  
University of Toronto  
Vector Institute  
kingsley@cs.toronto.edu

**Elliot Creager**  
University of Toronto  
Vector Institute  
creager@cs.toronto.edu

**Anna Goldenberg**  
University of Toronto  
Vector Institute  
anna.goldenberg@utoronto.ca

**David Duvenaud**  
University of Toronto  
Vector Institute  
duvenaud@cs.toronto.edu

## Abstract

Explanations of black-box classifiers often rely on saliency maps, which score the relevance of each input dimension to the resulting classification. Recent approaches compute saliency by optimizing regions of the input that maximally change the classification outcome when replaced by a *reference value*. These reference values are based on *ad-hoc* heuristics such as the input mean. In this work we *marginalize out* masked regions of the input, conditioning a generative model on the rest of the image. Our model-agnostic method produces realistic explanations, generating plausible inputs that would have caused the model to classify differently. When applied to image classification, our method produces more compact and relevant explanations, with fewer artifacts compared to previous methods.

## 1 Introduction

Neural networks achieve state-of-the-art performance in many domains, but their decisions are difficult to interpret. The lack of human-interpretable explanations of predictions of this expressive model class represents a serious impediment to their adoption in safety-critical areas like health care and autonomous driving [1]. Saliency maps are a tool for interpreting neural network classification that, given a particular input example and output class, score the relevance of each input dimension to the resulting classification. Recent works derived saliency maps by asking which input, if masked and filled in with an uninformative reference value, would change the classifier the most. Specifically, Fong and Vedaldi [2], Dabkowski and Gal [3] directly optimize the input mask over the entire image to maximize the change of classifier output. However, their choice of reference values are heuristic, *e.g.* blurring the image, using the mean of each color channel [2], or using random colors [3]. Since these strategies ignore the context of the surrounding pixels, they tend to produce unnatural in-filled images. If we think of a saliency map as interrogating the neural network classifier, then these approaches ask somewhat unusual questions, since the answers depend on how the classifier treats images outside of its training distribution. See Figure 1 for an example.

We instead would like our saliency map to answer the question: *Which region, when replaced by plausible alternative values, would most change the decision of the classifier?* We marginalize out the masked region, and use a generative model to infill, conditioning the generative model on the non-masked parts of the image.

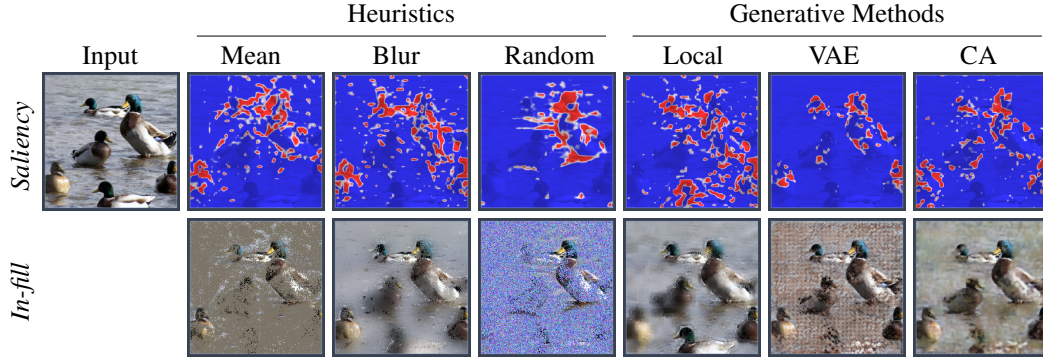


Figure 1: **Comparison of saliency maps and their corresponding reference values.** Each saliency map (top row) is the result of an optimization that seeks to change the classification outcome of an in-filled image (bottom row) by mixing the original image in the salient (red) regions and a reference image in the non-salient (blue) regions. We compare several methods for computing the reference during optimization, 3 heuristics and 3 generative in-filling models. We argue that the use of strong generative models—e.g., Contextual Attention GAN (CA) [5]—ameliorates artifacts and unnatural in-filled images characteristic of the heuristic methods that result in poor saliency maps.

In this paper, we make several contributions. First, we provide a new model-agnostic framework to visualize any differentiable classifier, based on variational Bernoulli dropout [4]. Second, we combine generative models with the new model-agnostic framework to produce saliency maps on ImageNet that better identify relevant and concentrated pixels compared with existing methods. Third, we propose a new way to quantitatively evaluate the quality of saliency maps using a generative model.

## 2 Related work

Gradient-based approaches [6, 7] derive a saliency map for a given input example and class target by computing the gradient of the classification probability (or softmax input) with respect to each component (e.g., pixel) of the input. However, the reliance on the local gradient information induces a bias due to gradient saturation or discontinuity in the DNN activations [8].

Reference-based approaches instead compute saliency according to how the output classification scores change when inputs are swapped with a reference value. For example, Shrikumar et al. [8] considers the reference as the background color (e.g., black in MNIST) and locally linearly approximates the classification difference before and after swapping the reference using an algorithm that resembles backpropagation. This method runs efficiently and addresses some problems of gradient discontinuity. However, the reliance on a heuristic reference is a drawback; it is not obvious how to select such a reference for datasets beyond MNIST. Also, the linear approximation ignores the nonlinear interactions among pixels.

Zintgraf et al. [9] computes the saliency of a component (or region of components, e.g., an image patch) by treating it as unobserved and marginalizing it out, then measuring the change in classification outcome. This probabilistic interpretation of imputation is attractive from a modeling perspective and yields qualitatively compelling saliency maps, but at great computational cost since the algorithm needs to iteratively marginalize out each pixel to compute the saliency map. Another potential downside is the failure to model interaction between components (pixels) in the classification [10]. Zintgraf et al. [9] use a large moving window to account for the interaction effects within that window, analyzing one window at a time. However, this approximation isn’t well suited to the case where multiple distant components or regions jointly support the resulting classification, or for non-image applications with arbitrary feature ordering.

Fong and Vedaldi [2] compute saliency by optimizing over perturbations that change the classification outcome. They express the perturbed input as a pixel-wise convex combination of the original input with a reference, and offer three heuristics for choosing the reference: mean input pixel value (typically gray), Gaussian noise, and blurred input. This approach is most closely related to ours,

which we discuss in section 3.2. Dabkowski and Gal [3] proposed a similar method but using random colors as reference values. In addition, rather than inferring their mask per image, they amortize the cost of inference by learning parameters of an auxiliary neural network that efficiently computes the saliency map at test time.

### 3 Proposed method

Dabkowski and Gal [3] proposed two objectives for optimizing the saliency map:

- Smallest deletion region (SDR) considers a saliency map as an answer to the question: *what is the smallest region of the input that could be swapped for (or mixed with) reference values such that the classification score is minimized?*
- Smallest supporting region (SSR) instead asks the question *what is the smallest region of the input that could be substituted into (or mixed with) the reference such that the classification score is maximized?*

Solving these optimization problems (which we formalize below) necessitates a reference value, which was previously chosen heuristically (e.g., mean pixel value per channel). We instead compute the saliency for each component by considering its imputation in a probabilistic framework [9, 11]. Here we describe such a framework for an image application where the input comprises pixels organized into regions, but our method is more broadly applicable to any domain where the classifier is differentiable.

Consider an input image  $\mathbf{x}$  with  $\mathbf{x}_{\setminus r}$  denoting that input with pixels from the region  $r$  removed (unobserved), class  $c$ , reference  $\hat{\mathbf{x}}$  and a classifier model  $\mathcal{M}$  with output probabilities  $p_{\mathcal{M}}(c|\mathbf{x})$ . The classifier output of the image with region  $r$  unobserved is expressed by marginalizing out  $x_r$ ,

$$p_{\mathcal{M}}(c|\mathbf{x}_{\setminus r}) = \mathbb{E}_{\mathbf{x}_r \sim p(\mathbf{x}_r|\mathbf{x}_{\setminus r})}(p_{\mathcal{M}}(c|\mathbf{x}_{\setminus r}, \mathbf{x}_r)). \quad (1)$$

We then approximate  $p(\mathbf{x}_r|\mathbf{x}_{\setminus r})$  by some generative model  $G$  (specific implementations are discussed in section 4.1) with distribution  $p_G(\mathbf{x}_r|\mathbf{x}_{\setminus r})$ . Then given a binary mask  $\mathbf{z}$  and the original image  $\mathbf{x}$ , we define an infilling function  $\phi$  as a convex mixture of the input and reference with binary weights,

$$\phi(\mathbf{x}, \mathbf{z}) = \mathbf{z} \odot \mathbf{x} + (\mathbf{1} - \mathbf{z}) \odot \hat{\mathbf{x}} \text{ where } \hat{\mathbf{x}} \sim p_G(\hat{\mathbf{x}}|\mathbf{z}=\mathbf{0}). \quad (2)$$

#### 3.1 Objective functions

SDR seeks a mask  $\mathbf{z}$  yielding low classification score when a small number of reference pixels are mixed into the mask regions. Specifically, given a classification score function  $s_{\mathcal{M}}(c|\mathbf{x})$  (discussed below), this is a minimization w.r.t  $\theta$  of

$$L_{SDR}(\theta) = \mathbb{E}_{q_{\theta}(\mathbf{z})} [s_{\mathcal{M}}(c|\phi(\mathbf{x}, \mathbf{z})) + \lambda \|\mathbf{z}\|_1]. \quad (3)$$

On the other hand, SSR aims to find a masked region that maximizes classification score while penalizing the size of the mask. For sign consistency with the previous problem, we express this as a minimization w.r.t  $\theta$  of

$$L_{SSR}(\theta) = \mathbb{E}_{q_{\theta}(\mathbf{z})} [-s_{\mathcal{M}}(c|\phi(\mathbf{x}, \mathbf{z})) + \lambda \|\mathbf{1} - \mathbf{z}\|_1]. \quad (4)$$

The classification score function  $s_{\mathcal{M}}(\cdot)$  represents the classification confidence; in our experiments we use the log-odds score of the in-class probability:

$$s_{\mathcal{M}}(c|\mathbf{x}) = \log p_{\mathcal{M}}(c|\mathbf{x}) - \log(1 - p_{\mathcal{M}}(c|\mathbf{x})) \quad (5)$$

Naively searching over all possible  $\mathbf{z}$  is exponentially costly in the number of pixels  $U$ . Therefore we specify a variational distribution over masks  $q_{\theta}(\mathbf{z})$  as a factorized Bernoulli

$$q_{\theta}(\mathbf{z}) = \prod_{u=1}^U q_{\theta_u}(z_u) = \prod_{u=1}^U \text{Bern}(z_u|\theta_u). \quad (6)$$

This corresponds to applying Bernoulli dropout [12] to the input pixels and optimizing the per-pixel dropout rate. We thus visualize  $\theta_u$  since it has the same dimensionality as the input. We call our

method FIDO because it uses a strong generative model (see section 4.1) to Fill-In the DropOut region.

To avoid unnatural artifacts, previous work [2, 3] included two regularization methods: upsampling and total variation penalization. Upsampling initializes  $\theta_u$  with smaller size of parameter (e.g.  $56 \times 56$ ) matrix, then upsamples it by bilinear interpolation to the whole image (e.g.  $224 \times 224$ ). Total variation penalty adds an  $\ell_2$  regularization penalty between  $\theta_u$  in adjacent pixels. To avoid losing too much signal from regularization, we use upsampling size 56 and no total variation effect unless otherwise mentioned. We show these two effects in the Supplementary sections A.1 and A.3.

To optimize the  $\theta$  through the discrete random mask  $z$ , we follow Gal et al. [13] in computing biased gradients via the Concrete distribution [14, 15]; we use temperature 0.1. We initialize all our dropout rates  $\theta$  to 0.5 since we find it increases the convergence speed and avoids trivial solutions. We optimize using Adam [16] with learning rate 0.05 and linearly decay the learning rate for 300 batches in all our experiments. Our PyTorch implementation takes about one minute on a single GPU machine to finish one image.

### 3.2 Comparison to Fong and Vedaldi [2]

The saliency map of Fong and Vedaldi [2], which we call Black Box Meaningful Perturbations (BBMP), can be seen as a special case of our method without a learned generative model. Instead of optimizing in expectation over the dropout distribution  $q_\theta(z)$ , Fong and Vedaldi [2] directly optimize SDR with  $z \in [0, 1]$ . We instead optimize the Bernoulli parameters of a discrete mask  $\{0, 1\}$ , which enables us to sample reference values  $\hat{x}$  conditioned on other non-dropped out ( $z = 1$ )  $x$ . In addition, our method can utilize mini-batches of samples  $z \sim q_\theta(z)$  to explore the huge space of masks more efficiently and get uncertainty estimates, while BBMP can only do a local search of the current single mask. We provide empirical comparison in Section 4.5.

## 4 Experiments

We first compare, both qualitatively and quantitatively, different infilling strategies, objectives, and network architecture used in our method FIDO. We also test FIDO’s stability and different regularization in supplementary A. Then we compare FIDO’s performance to the previous methods [2, 3]. Finally, we propose a new way to quantitatively evaluate all the saliency maps based on the generative models.

### 4.1 In-filling Methods

**Heuristic References** The **Mean** method sets the reference value as the per-channel mean value of the image. The **Blur** method generates reference value by blurring the input image with Gaussian kernel ( $\sigma = 10$ ) as proposed in Fong and Vedaldi [2]. The **Random** method follows Dabkowski and Gal [3] to generate a random constant color with small random Gaussian noise ( $\sigma = 0.2$ ).

**Generative Methods** We compare with three other methods that determine the reference value conditioned on the rest of the non-dropped images. **Local** method sets the reference value to be the average value of the surrounding non-dropped-out pixels during the optimization (we set that window to be  $15 \times 15$ ). **VAE** is an image completion Variational Autoencoder Iizuka et al. [17]. We found that using the predictive mean of the decoder network worked better than sampling. **CA** is the Contextual Attention GAN [5]. We use the pre-trained model provided by the authors.

Figure 2 demonstrates an example of how these six strategies infill a center mask of the image. The generative approaches (VAE and CA) perform visually sharper images than four other baselines. We also quantitatively evaluate these infilling strategies in the Supplementary A.

### 4.2 Comparisons between SSR and SDR objectives

Here we examine the choice between SDR and SSR objectives. Figure 3 qualitatively compares the performance of a variety of in-filling methods under each objectives. We find SDR objective leads to more artifacts and fragmented explanations than SSR objective, especially when a weak in-filling method (Mean) is used. We suspect this is due to the fact that while it is hard to find an infill value



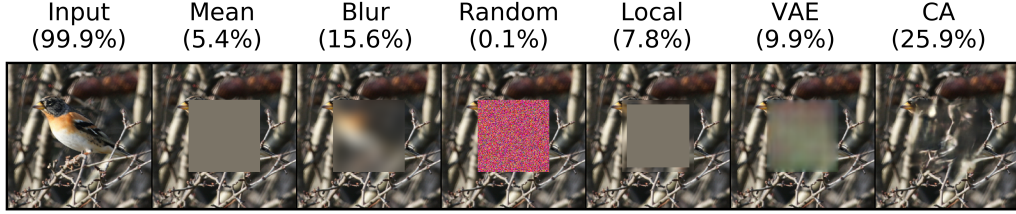


Figure 2: **Visualization of reference value infilling methods under centered mask.** The ResNet output probability of the correct class is shown for each imputed image.

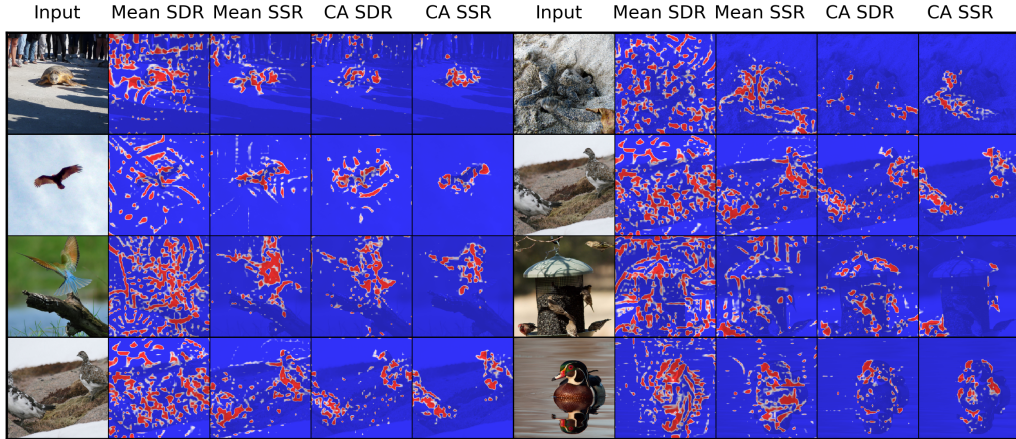


Figure 3: **Visualization of the effect of SSR objective versus SDR objective** using ResNet. The classifier gives correct predictions for all the images. We show the saliency map of SSR and SDR objectives under 2 infilling methods: Mean and CA. Here the red means important and blue means non-important. We find that SSR objective gives more concentrated explanations to the target, while SDR objective causes more artifacts around the object.

that increases the probability of the target class, it is much easier for the infill value to increase the probability of one of the other 999 classes by chance. To mitigate the effect of artifacts in the saliency masks, We evaluate all our images under the SSR objective for the rest of the experiments.

### 4.3 Comparisons between different infilling methods

Here we demonstrate the merits of using strong generative model that produces substantially fewer artifacts and a more concentrated saliency map. In Figure 4, we generate saliency maps of different infilling techniques by interpreting ResNet under SSR objective with sparsity penalty  $\lambda = 10^{-3}$ . We observed a susceptibility of the heuristic in-filling methods (Mean, Blur, Random) to artifacts in the resulting saliency maps. While the Mean method tends to produce fragmented artifacts around the object, Blur and Random find unexpected blobs and lines around edge, perhaps fooling edge filters in the low level of the network. On the other hand, generative in-filling (Local, VAE, CA) tends to produce fewer artifacts, presumably because it forces the in-filled image to be closer to the natural image manifold of the training data. Subjectively speaking, CA in-filling tends to produce the fewest number of artifacts while capturing the main properties of the class instance within the image.

To quantify the artifacts each method produces, we calculate the ratio of the MAP saliency mask outside of the bounding box as our proxy to measure the quality of the saliency map and the degree of artifacts. This is computed as the proportion of  $\theta < 0.5$  (not dropped out in the MAP configuration) outside of the bounding box. In Figure 5, we show the ratio for the six infilling methods. We demonstrate that generative model CA produces the fewest artifacts.

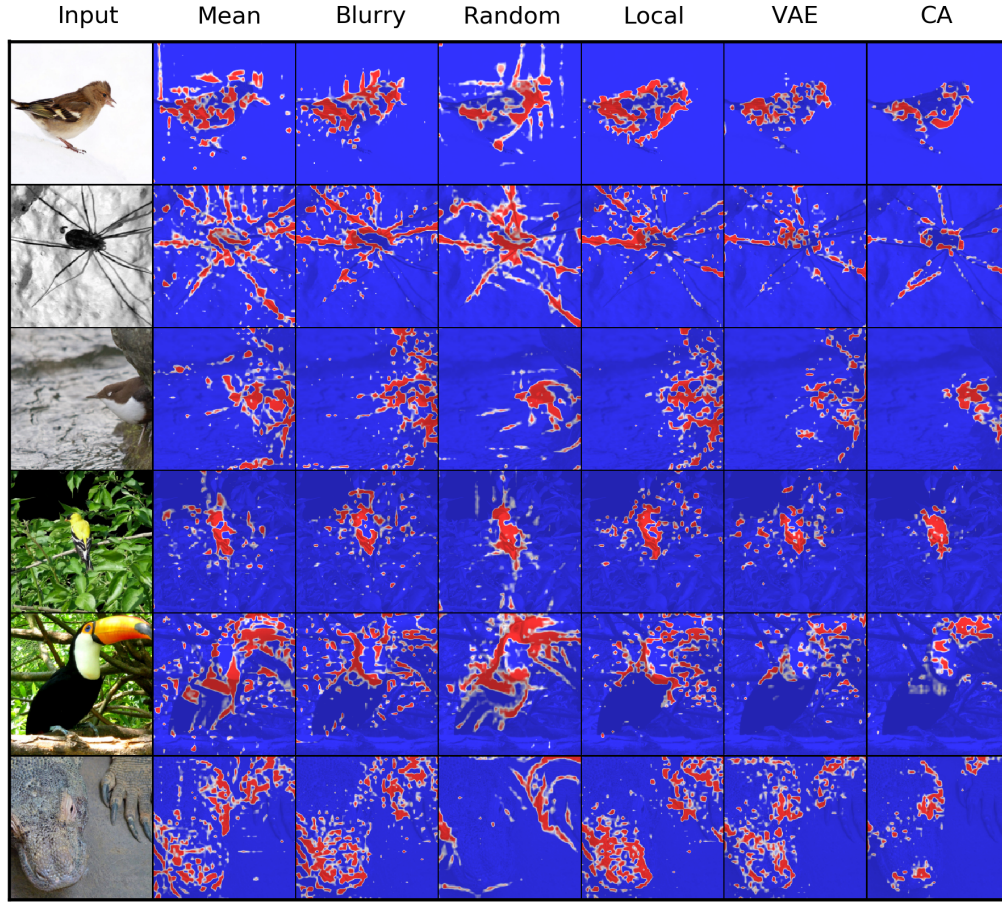


Figure 4: **Comparison of saliency map under different infilling methods** by SSR using ResNet. Heuristics baselines (Mean, Blur and Random) tend to produce more artifacts, while generative approaches (Local, VAE, CA) produce more focused explanations on the targets.

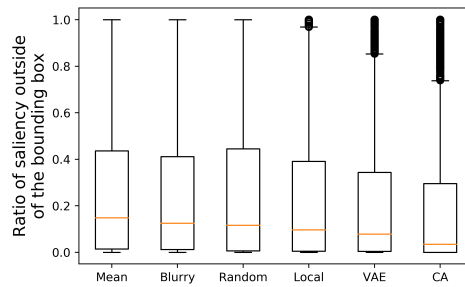


Figure 5: **Box plot of the saliency map ratio outside of the bounding box** for different infilling methods using ResNet for 1, 971 images. The lower the better.

#### 4.4 Network Comparisons

We can use saliency maps to investigate how different neural network architectures prioritize different regions of the input space for a particular classification. We test three network architectures: AlexNet, VGG and ResNet under CA methods and show the results in Figure 6. All the network classifies examples correctly. We observe that AlexNet generally produces more fragmented explanations. Also, different architectures appear to focus on slightly different input areas. For example in the last image, we can see AlexNet focuses more in the body region of the bird, while Vgg and ResNet focus on the head.

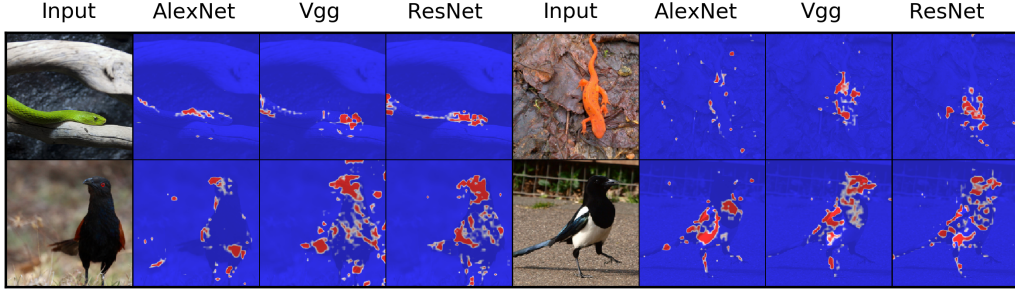


Figure 6: **Comparison of visualization across different network architectures.** We compare 3 different networks: AlexNet, Vgg and ResNet. (Using CA infilling method and  $\lambda = 10^{-3}$ )

#### 4.5 Comparisons of BBMP and FIDO

Here we compare FIDO with two previously proposed methods, BBMP with Blur in-filling strategy [2] and BBMP with Random in-filling strategy [3]. One potential concern in qualitatively comparing these methods is that each method might have a different sensitivity to the sparsity parameter  $\lambda$ . Subjectively, we observe that BBMP requires roughly 5 times higher sparsity penalty  $\lambda$  to get visually comparable saliency maps. In our comparisons we sweep  $\lambda$  over a reasonable range for each method and show the resulting sequence of increasingly sparse saliency maps (Figure 7).

We use  $1e-3$ ,  $2e-3$ ,  $5e-3$  and  $0.01$  for BBMP methods and  $2e-5$ ,  $5e-4$ ,  $1e-3$  and  $2e-3$  for FIDO. We observe that all methods are prone to artifacts in the low  $\lambda$  regime, so the appropriate selection of this value is clearly important. Interestingly, BBMP Blur and Random respectively find artifacts with different quality: small patches and pixels for Blur and structure off-object lines for Random. FIDO with CA is arguably the best saliency map, producing fewer artifacts and concentrating saliency on small regions for the images.

#### 4.6 Quantitative Evaluations

To quantitatively compare the saliency maps, we follow Fong and Vedaldi [2], Shrikumar et al. [8] to examine how the most important pixels (ranked by saliency) affect the classification outcome. That is, removing pixels from a ‘better’ saliency map in the order of the most saliency region to the least, should result in a greater loss (to the score) given the same number of pixels removed compared to a worse saliency map; we use CA to in-fill the removed pixels. To standardize score loss across images, we use the ratio of the loss in score of the target pixel removal normalized by the loss in score if we remove all the pixels. In Figure 8, we test 763 validation images correctly predicted by ResNet and use our scoring procedure to evaluate the number of pixels needed to result in score drop by a given percentage (the lower (smaller) is the number of pixels needed to be removed, the better). We evaluate FIDO along with all the baselines with all the in-filling strategies as well as BBMP with Blur and Random in-filling strategies. Here we choose FIDO with  $\lambda = 1e-3$  and BBMP with  $\lambda = 5e-3$  since they produce visually similar number of red regions (see section 4.5). We show that FIDO with CA is the best in terms of using fewer pixels to get the same log-odds ratio change in a large range of scenarios. We also find that our generative infilling approaches (Local, VAE and CA) are overall better than the heuristics methods Mean, Blur and Random, which is consistent with our qualitative comparisons.



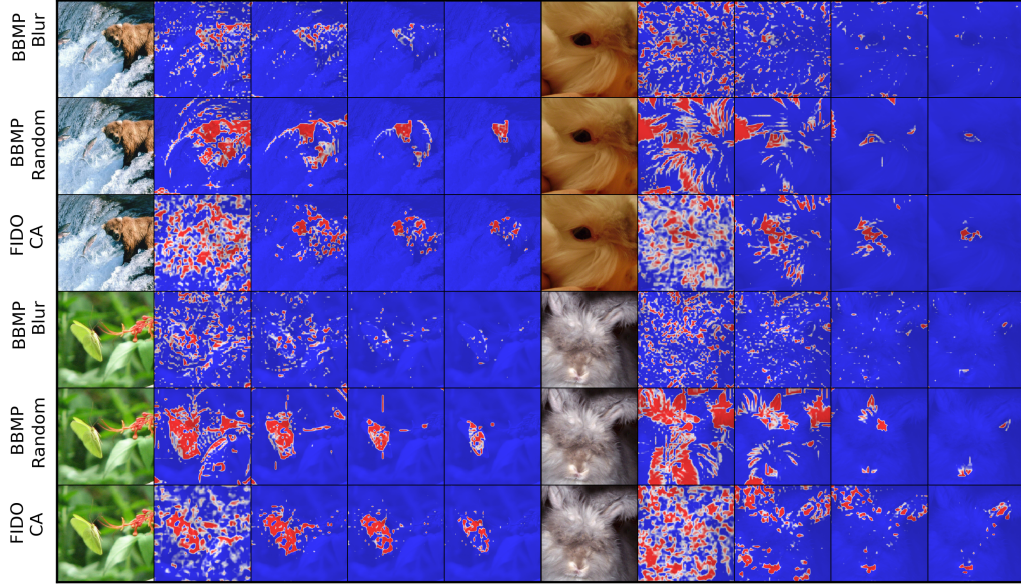


Figure 7: **BBMP vs FIDO saliency map** by increasing the sparsity penalty  $\lambda$  value from left to right. We compare with BBMP under Blur and Random, and FIDO under CA in-filling strategies. Note that here BBMP and FIDO methods use different  $\lambda$  (see main text for details). We show the heuristics produce more artifacts (BBMP Blur) or produces weird lines (BBMP Random) compared to our method.

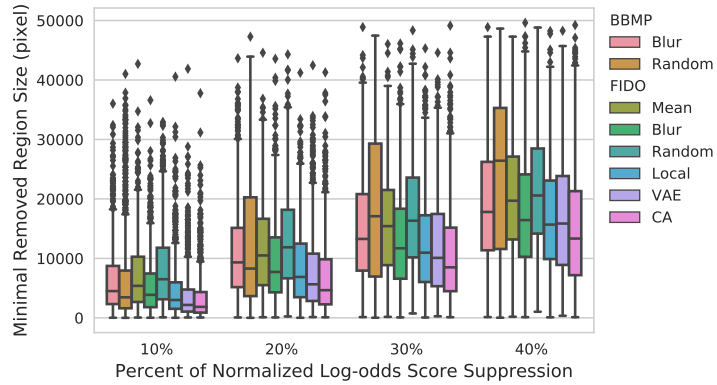


Figure 8: Comparisons of different saliency maps which requires minimal size of mask that suppresses the normalized score. We compare all our infilling methods under our strongest generative model CA. Here we choose  $\lambda = 5e-3$  for BBMP and  $1e-3$  for FIDO. The lower the better.

## 5 Conclusion

We proposed FIDO, a new saliency map for differentiable classifiers that uses adaptive Bernoulli dropout with generative in-filling of the dropped-out inputs, combining the best properties of recently proposed methods [2, 3, 9]. We also made explicit the role of imputation by a generative model and compared various in-filling approaches, both heuristic and generative, to conclude that generative models produce more interpretable explanations and fewer artifacts. Finally, we proposed a way to use generative models to quantitatively evaluate the performance of saliency maps.

## References

- [1] Menaka Narayanan, Emily Chen, Jeffrey He, Been Kim, Sam Gershman, and Finale Doshi-Velez. How do humans understand explanations from machine learning systems? an evaluation of the human-interpretability of explanation. *arXiv preprint arXiv:1802.00682*, 2018.
- [2] R. Fong and A. Vedaldi. Interpretable explanations of black boxes by meaningful perturbation. In *Proceedings of the International Conference on Computer Vision (ICCV)*, 2017.
- [3] Piotr Dabkowski and Yarin Gal. Real time image saliency for black box classifiers. *arXiv preprint arXiv:1705.07857*, 2017.
- [4] Yarin Gal and Zoubin Ghahramani. Dropout as a bayesian approximation: Representing model uncertainty in deep learning. In *international conference on machine learning*, pages 1050–1059, 2016.
- [5] Jiahui Yu, Zhe Lin, Jimei Yang, Xiaohui Shen, Xin Lu, and Thomas S Huang. Generative image inpainting with contextual attention. *arXiv preprint arXiv:1801.07892*, 2018.
- [6] Karen Simonyan, Andrea Vedaldi, and Andrew Zisserman. Deep inside convolutional networks: Visualising image classification models and saliency maps. *arXiv preprint arXiv:1312.6034*, 2013.
- [7] Ramprasaath R Selvaraju, Abhishek Das, Ramakrishna Vedantam, Michael Cogswell, Devi Parikh, and Dhruv Batra. Grad-cam: Why did you say that? *arXiv preprint arXiv:1611.07450*, 2016.
- [8] Avanti Shrikumar, Peyton Greenside, and Anshul Kundaje. Learning important features through propagating activation differences. *arXiv preprint arXiv:1704.02685*, 2017.
- [9] Luisa M Zintgraf, Taco S Cohen, Tameem Adel, and Max Welling. Visualizing deep neural network decisions: Prediction difference analysis. *arXiv preprint arXiv:1702.04595*, 2017.
- [10] Marco Ancona, Enea Ceolini, Cengiz Öztireli, and Markus Gross. Towards better understanding of gradient-based attribution methods for deep neural networks. *arXiv preprint arXiv:1711.06104*, 2017.
- [11] M. Robnik-Šikonja and I. Kononenko. Explaining Classifications For Individual Instances. *IEEE Transactions on Knowledge and Data Engineering*, May 2008.
- [12] Nitish Srivastava, Geoffrey E Hinton, Alex Krizhevsky, Ilya Sutskever, and Ruslan Salakhutdinov. Dropout: a simple way to prevent neural networks from overfitting. *Journal of machine learning research*, 15(1):1929–1958, 2014.
- [13] Yarin Gal, Jiri Hron, and Alex Kendall. Concrete dropout. *arXiv preprint arXiv:1705.07832*, 2017.
- [14] Chris J Maddison, Andriy Mnih, and Yee Whye Teh. The concrete distribution: A continuous relaxation of discrete random variables. *arXiv preprint arXiv:1611.00712*, 2016.
- [15] Eric Jang, Shixiang Gu, and Ben Poole. Categorical reparameterization with gumbel-softmax. *arXiv preprint arXiv:1611.01144*, 2016.
- [16] Diederik Kingma and Jimmy Ba. Adam: A method for stochastic optimization. *arXiv preprint arXiv:1412.6980*, 2014.
- [17] Satoshi Iizuka, Edgar Simo-Serra, and Hiroshi Ishikawa. Globally and Locally Consistent Image Completion. *ACM Transactions on Graphics (Proc. of SIGGRAPH)*, 36(4):107, 2017.



## A Further analysis

### A.1 Upsampling Effect

To motivate our choices of upsampling size of 56 for the rest of the experiments, we show the effects of different upsampling sizes. In Figure 9, we demonstrate two examples with different upsampling size under Mean and CA infilling methods with SSR objectives. We show that the weaker infilling strategy Mean requires stronger regularization to avoid artifacts compared to CA. Note that although CA produces much less artifacts compared to Mean, it still produces some small artifacts outside of the objects which is unfavored. We then choose 56 for the rest of our experiments to balance between details and the removal of the artifacts.

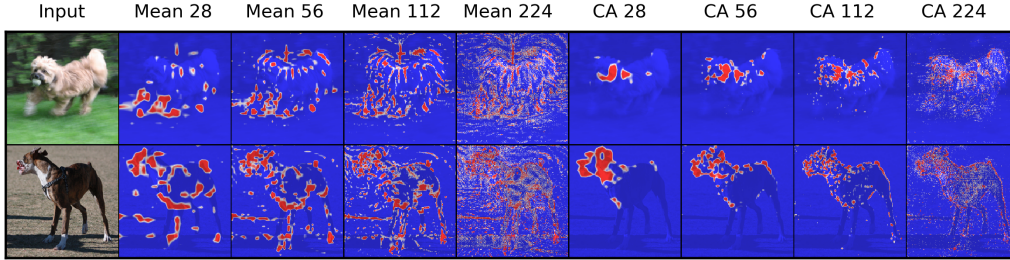


Figure 9: **Comparisons of upsampling effect** in Mean and CA infilling methods. We show the upsampling regularization removes the artifacts especially in the weaker infilling method Mean.

### A.2 Stability

To show the stability of our method, we test our method with different random seeds and observe if they are similar. In Figure 10, our method produces similar saliency map for 4 different random seeds.

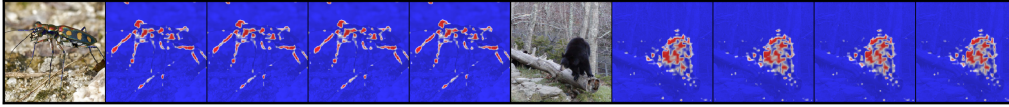


Figure 10: **Testing the stability of our method** with 4 different random seeds. They produce similar saliency maps. (Using CA infilling method with ResNet and  $\lambda = 10^{-3}$ )

### A.3 Total Variation Effect

Although we do not include total variation smoothing prior in our experiments, we still test the effect of total variation regularization in Figure 11. We find the total variation can reduce the adversarial artifacts further, while risking losing signals when the total variation penalty is too strong.

### A.4 Analysis of generative model infilling

Here we quantitatively compare the in-filling strategies. The generative approaches (VAE and CA) perform visually sharper images than four other baselines. Since we expect this random removal should not remove the target information, we use the classification probability of the ResNet as our metric to measure how good the infilling method recover the target prediction. We quantitatively evaluate the probability for 1,000 validation images in Figure 12. We find that VAE and CA consistently outperform other methods, having higher target probability. We also note that all the heuristic baselines (Mean, Blur, Random) perform much worse since the heuristic nature of these approaches, the images they generate are not likely under the distribution of natural images leading to the poor performance by the classifier.

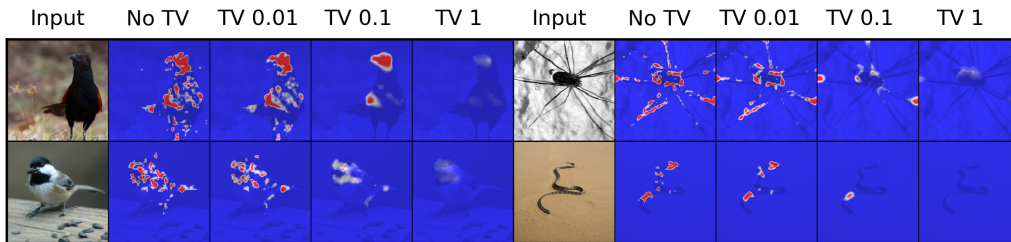


Figure 11: **Total Variation Regularization Effect.** We show the saliency maps of 4 increasing total variation (TV) regularization. We show that strong regularization risks removing signal.

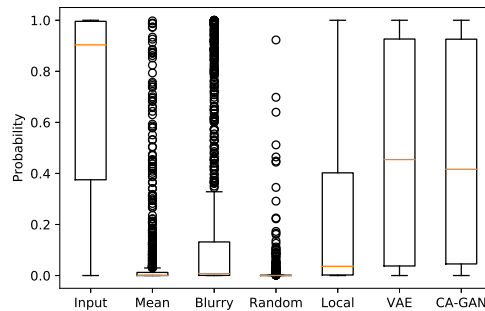


Figure 12: **Box plot of the classifier probability under different infilling with respect to random masked pixels** using ResNet under 1000 images. We show that generative models (VAE and CA) performs much better in terms of classifier probability.